INTERFACE CRACK GROWTH UNDER TRANSVERSE COMPRESSION: NEARBY FIBRE EFFECT

C. Sandino, E. Correa and F. París

Group of Elasticity and Strength of Materials, Continuum Mechanics Department, School of Engineering - Universidad de Sevilla, Camino de los Descubrimientos s/n 41092 Sevilla, Spain
Email: ecorrea@us.es

Keywords: Micromechanics, Interfacial Fracture Mechanics, Transverse Cracking, BEM Analysis, Compression.

Abstract
The influence of the presence of an undamaged fibre on the interface crack growth associated with the inter-fibre failure under uniaxial compression is studied by means of a two-fibre BEM model, in order to analyse the alterations brought about by the variation of the position of the undamaged fibre with reference to a single-fibre case, using Interfacial Fracture Mechanics concepts. The results obtained reveal that when the secondary fibre is approximately aligned with the position of the appearance of the failure or at 120º from it, the presence of the secondary fibre promotes the initiation of the interface crack growth, whereas for the rest of the positions, it provokes an inhibition of the failure. In addition, the influence of the presence of friction between the crack faces is also discussed in order to obtain a more accurate prediction of the end of the unstable growth of the interface crack.

1. Introduction

The damage mechanism known as matrix/inter-fibre failure (occurring in fibrous composite materials submitted to loads perpendicular to the direction of the fibres) has already been the object of several studies by Correa et al. [1-3] for composite materials under compression transverse to the fibres. These studies assume the hypothesis that transverse failure starts with small debonds appearing at the fibre-matrix interfaces, allowing the micromechanical stages of the matrix/inter-fibre failure under uniaxial compression to be identified: (1) the appearance of the damage in the form of a 'bubble' at 45º from the direction of the external load, the position of the maximum value of the shear stress; (2) the growth along the interface from the lower crack tip until the crack reaches a certain length (where the closing of the 'bubble' occurs); (3) the cracks kinking into the matrix, leading to the macro failure as a result of the coalescence between different cracks.

This study is focused on the second stage of the mechanism of damage under compression; a two-fibre BEM model is developed in order to evaluate the alterations brought about by the presence of an undamaged nearby fibre on the evolution of an interface crack between a primary central fibre and the matrix, in relation to the results of a single-fibre model and in a similar way to the approach employed by Sandino et al. [4, 5] for uniaxial and biaxial tension respectively. Interfacial Fracture Mechanics concepts, Mantič et al. [6], are used for the analysis of the results. In addition, the influence of the presence of friction between the crack faces together with the growth occurring at both crack tips is also discussed.

2. Numerical Model

In order to study the second stage on the damage mechanism, a numerical model was implemented using a tool based on BEM and implemented by Graciani et al. [7]. This BEM tool was especially developed for solving plane elastic problems for contact and interface cracks in planar problems and in axisymmetric problems. Fig. 1 represents this model, which considers an incipient interface crack located at 45º from the direction of the external unitary compressive load σ_0 (position of the maximum value of the shear stress at the interface) in the presence of a undamaged secondary fibre, the crack growing along the matrix-fibre interface under the plane strain hypothesis. Solid 'M' represents the matrix and Solids 'PF' and 'SF' the primary and secondary fibres respectively. The dimensions of the model are defined by r_1, which represents the radius of the fibres (r_1=7.5·10^{-6}m), and a, b representing the dimensions of the matrix (the boundary effect is avoided by imposing the condition a=b=100r_1, the matrix being large enough). The materials considered correspond to a glass fibre-epoxy matrix system whose elastic properties are defined in [1]. The relative position between both fibres is defined by the parameters r_2 and θ_2, their values being modified in order to create the different cases under consideration. Assuming hexagonal packing, the initial value of the distance between the fibres (r_2^0) corresponds to a fibre volume fraction of 75%.

The problem can be characterised from the Fracture Mechanics point of view by using the Energy Release Rate, G. This value can be determined by applying an expression based on the Virtual Crack Closure Technique (VCCT) [8], included in [1]. Dimensionless results for G will be calculated, following Toya [9] and Murakami [10], by dividing the values of G by G_0:

$$G_0 = \left(\left(1+\kappa^m\right)/8\mu^m\right)\sigma_0^2 r_1 \pi \tag{1}$$

where κ^m=3-4ν^m, μ^m is the shear modulus of the matrix and σ_0 is the applied external compression.

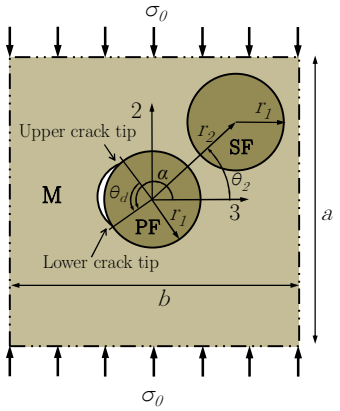

Figure 1. Model representing an interface crack at the primary fibre in the presence of an undamaged secondary fibre.

3. Energy Release Rate

G versus α (position of the lower crack tip) can be calculated, considering an initial crack of θ_d=10º (θ_d being the debonding angle, see Fig. 1) symmetric to the position α=135º and assuming the hypothesis that the crack grows from the lower tip [1]. For r_2^0, a selection of values of θ_2 and the debonding range 10º≤θ_d≤100º, G is represented in Fig. 2. The single-fibre case, also included as a reference, coincides with the results presented in [1].

It can be seen that, for $\alpha \leq 195^o$ ($\alpha=195^o$ being the position of the minimum G value for the single-fibre case) and the ranges $0^o \leq \theta_2 \leq 45^o$, $120^o \leq \theta_2 \leq 180^o$ and $225^o \leq \theta_2 \leq 285^o$, G evolution stands higher than the level established by the reference case for all or the main part of the α range under consideration. For the rest of the θ_2 values, G remains below the single-fibre case. From $\alpha=195^o$ onwards, G evolution stands above the reference level for the ranges $315^o \leq \theta_2 \leq 15^o$, $75^o \leq \theta_2 \leq 120^o$ and $180^o \leq \theta_2 \leq 240^o$, and below this level for the rest of the positions of the secondary fibre. As can be observed, for the range $165^o \leq \theta_2 \leq 195^o$, G evolution presents important qualitative changes in terms of the shape of the curve, suggesting the need of a more detailed analysis of Modes I and II of fracture.

The G value associated with the damage initiation (i.e. $G(\alpha=140^o)$, the value of G associated with the first debond considered $\theta_d=10^o$) can be considered as a relevant parameter for the damage mechanism at the micromechanical level [4,5], because it allows a connection between the micromechanical and macromechanical levels to be established. In particular, when this value is higher than the reference case (single-fibre), the crack starts to propagate at a lower level of load; the presence of the secondary fibre involving an accelerative effect against failure. On the contrary, when $G(\alpha=140^o)$ is lower than the single-fibre value, a higher level of load is needed to initiate the crack growth. Accordingly, the secondary fibre represents a protective effect against failure. Regarding the obtained results, Fig. 3 summarises the effects of the presence of the secondary fibre against failure for the whole θ_2 range. The strongest protective effect is found for $\theta_2=75^o$, $G(\alpha=140^o)$ being 60% lower with reference to the single-fibre case, whereas for $\theta_2=120^o$ the highest accelerative effect is obtained, since $G(\alpha=140^o)$ is 107% higher than in the single-fibre case. It is important to remark that, in view of Fig. 3, the θ_2 ranges corresponding to the protective and accelerative effects define an approximate rotational symmetry each 120^o from the position of the first debond of the crack.

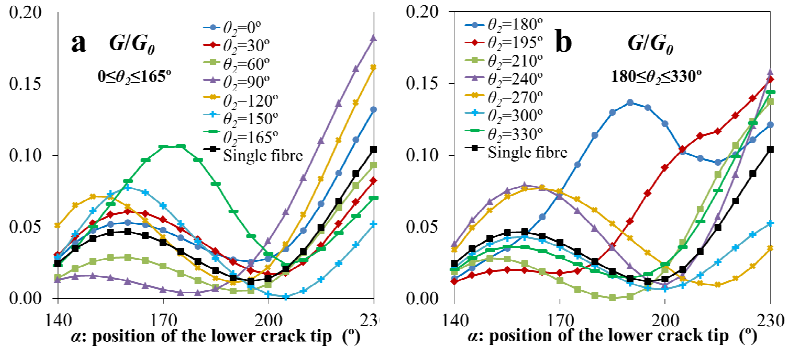

Fig. 2. Energy Release Rate, G, versus α: (a) $0^o \leq \theta_2 \leq 165^o$, (b) $180^o \leq \theta_2 \leq 330^o$

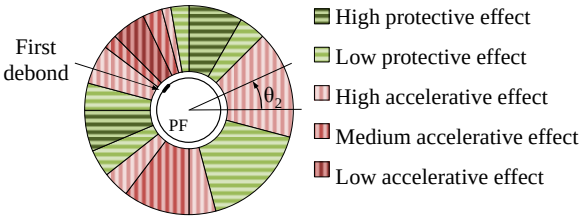

Fig. 3. θ_2 -ranges effect of the secondary fibre on the initiation of the interface crack growth.

Regarding Modes I and II, G_I and G_{II} are plotted versus α in Figs. 4 and 5 respectively for the whole θ_2 range and the single fibre case. G_I stays above the single-fibre case for the ranges $345^o \leq \theta_2 \leq 30^o$, $165^o \leq \theta_2 \leq 195^o$ and $240^o \leq \theta_2 \leq 270^o$, this fact suggesting the presence of greater sizes of the 'bubble'. This

matter is especially relevant for the range $165^o \leq \theta_2 \leq 195^o$, since G_I reaches considerably higher values than in the reference case, as could be expected in view of the approximate alignment of the secondary fibre with the position where the maximum radial relative displacements between the crack faces are expected, thus amplifying these displacements. For the positions $60^o \leq \theta_2 \leq 105^o$, $\theta_2=225^o$ and $300^o \leq \theta_2 \leq 315^o$, G_I remains below the single-fibre case and for $\theta_2=210^o$ G_I is negligible. With regard to the disappearance of Mode I, it is advanced for $60^o \leq \theta_2 \leq 120^o$ and $\theta_2=225^o$ in relation to the reference case and delayed for $0^o \leq \theta_2 \leq 30^o$, $165^o \leq \theta_2 \leq 195^o$ and $255^o \leq \theta_2 \leq 285^o$, which may be related to the delay or advance of the appearance of a finite contact zone. With reference to G_{II}, no remarkable qualitative changes are observed, except a slightly variation of position of the minimum: advanced for $60^o \leq \theta_2 \leq 120^o$, $165^o \leq \theta_2 \leq 210^o$ and $315^o \leq \theta_2 \leq 0^o$, and delayed for $135^o \leq \theta_2 \leq 150^o$ and $240^o \leq \theta_2 \leq 285^o$.

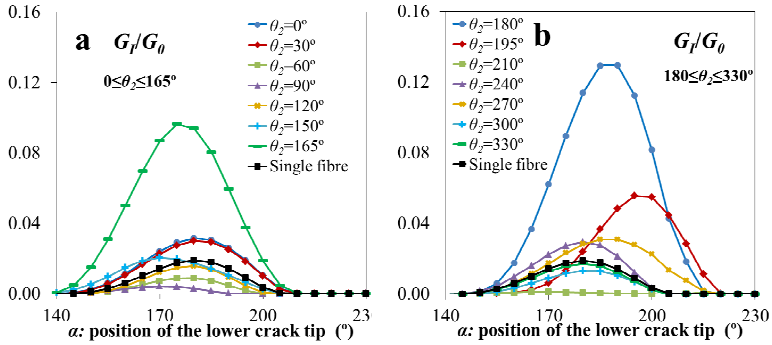

Fig. 4. Mode I component of the Energy Release Rate, G_I , versus α: (a) $0^o \leq \theta_2 \leq 165^o$, (b) $180^o \leq \theta_2 \leq 330^o$

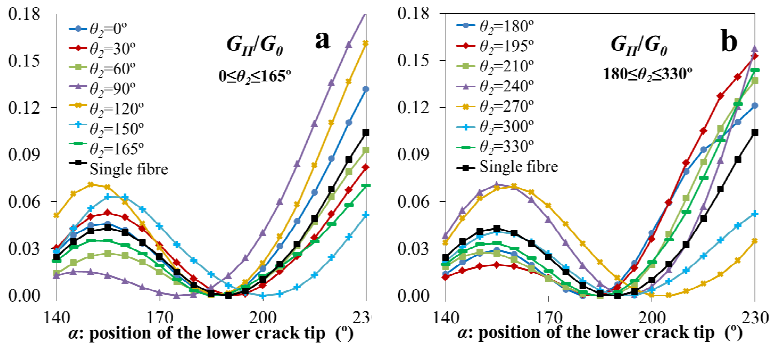

Fig. 5. Mode II component of the Energy Release Rate, G_{II}, versus α: (a) $0^o \leq \theta_2 \leq 165^o$, (b) $180^o \leq \theta_2 \leq 330^o$

4. Propagation of the Interface Crack

The end of the interface crack unstable growth can be predicted by comparing the G evolution with an estimation of the critical value of the Energy Release Rate, G_c. The estimation of the G_c taken into consideration is based on the proposal by Hutchinson and Suo [11], in the same way as detailed in [1]:

$$G_c(\psi_k) = G_{1c}\left[1+\tan^2\left[(1-\lambda)\psi_k\right]\right] \tag{2}$$

where G_{1c} represents the critical value of G_c for Mode I (it is calculated following [1]). G_{1c} value has been chosen to make $G_c(\alpha=140^o)$ coincide with $G(\alpha=140^o)$ for each of the values of θ_2 considered. λ is the fracture mode sensitivity parameter ($\lambda=0.25$, in this study) and ψ_k is the local phase angle, which represents the evolution of the fracture mode mixity and can be obtained following [12].

Figs. 6a and b show the G and G_c evolutions for two representative cases, θ_2=15º and θ_2=210º, also including the single-fibre case. It can be observed that, for θ_2=15º the crack extends towards larger positions of the lower crack tip (α≈215º) than in the reference case (α≈210º). Conversely, for θ_2=210º the unstable growth reaches a smaller length (α≈175º). To summarise, Fig. 6c represents the comparison of the estimation of the end of the unstable growth for the whole θ_2 ranges in relation to the single fibre case. The largest lengths of unstable growth are predicted when the position of the secondary fibre is approximately perpendicular to the direction of the compressive load, whereas the shortest ranges are obtained for 75º≤θ_2≤90º (approximately aligned with the direction of the load) and for θ_2=210º (the crack grows under Mode II along the entire propagation). The positions implying the largest θ_d ranges of unstable growth are related to the observations made in Section 3 about higher levels of G_I and the delay of the appearance of the contact zone at the lower crack tip. Conversely, the shortest θ_d ranges of unstable growth are attributed to lower levels of G_I and the advance of the appearance of the contact zone. A more accurate prediction for the end of the unstable growth could be obtained considering the presence of friction in the analysis; this work is developed in Section 6.

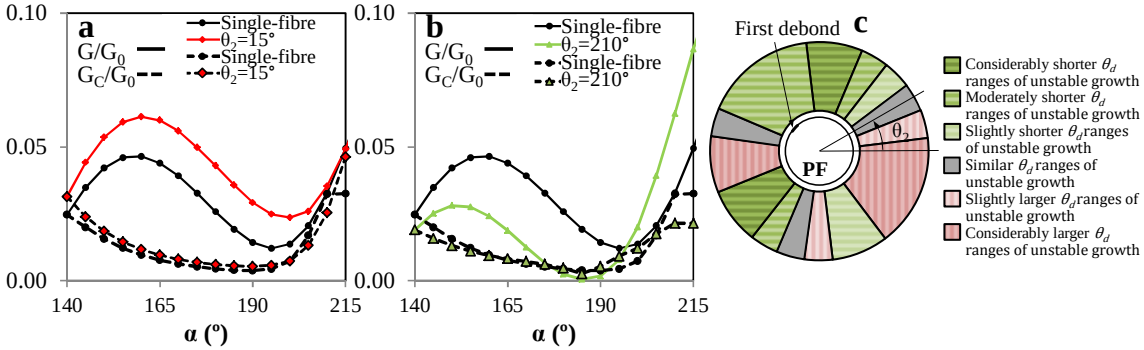

Fig. 6. Comparison between G and G_c versus α for (a) θ_2=15º, (b) 210º; (c) Graph representing the effects of the secondary fibre on the unstable growth.

5. Effect of the Increase on the Inter-Fibre Spacing

The study of the increase of the inter-fibre spacing allows an r_2 value, from which the effects of the secondary fibre are negligible, to be established. The same approach of the previous sections was implemented for increasing r_2 cases and it was observed that the influence of the presence of the secondary fibre on the second stage of the damage mechanism remains until r_2/r_2^0=4. When compared with the tensile uniaxial case [4], it is observed that, for this compressive uniaxial study the distance needed to make the results coincide with those of the single-fibre model is significantly lower (in particular, the distance is approximately one half of that obtained in [4].)

6. Influence of Friction under Transverse Compression

The important role that Mode II propagation and the corresponding appearance of contact zones at the crack tips play in the second stage of the matrix failure at micromechanical level, reveals the need of taking into consideration the presence of friction due to the roughness existing at the crack faces, in order to achieve a better understanding of the damage mechanism and a more accurate prediction of the end of the unstable growth. For this purpose, a numerical analysis of the effect produced by the presence of frictional contact on the propagation of the interface crack can be carried out by using the single-fibre and two-fibre BEM models employed in the previous sections. The BEM tool developed by Graciani [7] allows the frictional contact to be taken into consideration; in this study, a friction coefficient c_f=0.5 was chosen.

The Energy Release Rate can also be calculated using a revised version of the equation presented in [1], adding the effect of friction. In particular, a new fracture parameter is employed in this section, $\hat{G}$, following the equation proposed by Graciani et al. in [13], which adds a new term that represents the Mode II component associated with the crack propagation assuming friction between the crack lips. All $\hat{G}$ values were divided by G_0 (Eq. 1) in order to obtain dimensionless results.

The evolution of the frictional Energy Release Rate can now be compared with the results obtained in Section 3 for the single-fibre case, Fig. 7 representing the G, $\hat{G}$ and their corresponding Mode I and Mode II components (G_I, G_{II}, $\hat{G}_I$ and $\hat{G}_{II}$) versus α (position of the lower crack tip), for the range $10^o \leq \theta_d \leq 100^o$. As can be observed, friction causes a decrease on the $\hat{G}$ level, altering both modes of fracture. However, as could be expected, friction alters more considerably the α subranges where the interface crack is dominated by Mode II. This is especially significant for $\alpha \geq 206^o$, as the contact zone starts to develop at the lower crack tip. It is also observed that friction does not produce relevant alterations on the appearance and disappearance of both modes of fracture.

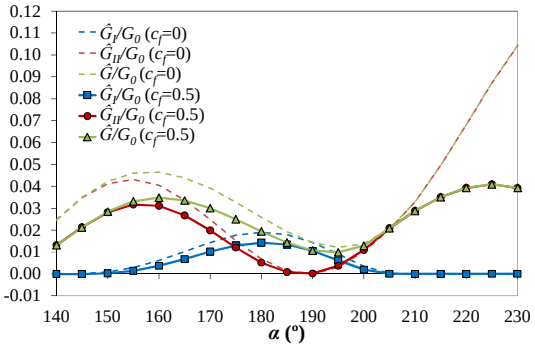

Fig. 7. $\hat{G}_I$, $\hat{G}_{II}$ and $\hat{G}$ versus α, for the single-fibre case (c_f=0, 0.5).

In [1] the authors concluded that the hypothesis of propagation at the lower crack tip was more favourable than at the upper crack tip due to the energetic comparison and the open configuration of the crack ('bubble') at the lower crack tip. Nevertheless, in this section the possibility that the interface crack grows at both crack tips at each step of growth is taken into consideration, due to the important decrease on the $\hat{G}$ produced where the lower contact zone is supposed to develop ($\alpha \geq 206^o$).

For this purpose the ratio $\hat{G}/\hat{G}_c$ ($\hat{G}_c$ is obtained using Eq. 2) is calculated for both crack tips. The interface crack starts to propagate at its lower crack tip, since the ratio is greater than that obtained for the upper crack tip. This situation is maintained until θ_d=70º, this position coinciding with the disappearance of the propagation on mixed mode at the lower crack tip and the appearance of a finite contact zone. From this position onwards, the crack alternates lower and upper crack tip growth ranges, until the end of the unstable growth is achieved at θ_d=140º. This prediction is made by assuming that the unstable growth ends when $\hat{G}/\hat{G}_c$<1 at one of the crack tips. The final deformed configuration of the primary fibre for single-fibre case is plotted in Fig. 8. In order to correctly visualise this deformed configuration, it was necessary to employ a factor of 10^5 on the interface displacements.

This approach was also used for the two-fibre model, taking into consideration the same θ_2 ranges that were employed in the previous sections. As can be observed in Fig. 8, in view of the final deformed configuration for different positions of the secondary fibre, the shortest lengths of unstable growth and the smallest sizes of the 'bubble' are obtained when the secondary fibre lies within the ranges $120^o \leq \theta_2 \leq 150^o$ and $210^o \leq \theta_2 \leq 240^o$. These ranges are approximately aligned with the zones where the upper and lower contact zones are expected to develop in the single-fibre case. The most extreme

situation is found for the θ_2=210º case, where the entire propagation is produced in pure Mode II and, consequently, the 'bubble' does not develop, which means that both crack lips are in contact, the presence of friction hindering the propagation. This effect was already observed for the non-frictional case (Section 4). Conversely, when the secondary fibre is located at 90º from the direction of the external load (θ_2=0º, 180º), the opposite effect is observed. The secondary fibre is aligned with the zones where the 'bubble' is expected to develop, in view of the results of the single-fibre case. This situation amplifies considerably the size of the 'bubble' and makes the crack grow until greater values of θ_d (with reference to the single-fibre case). This situation was also observed in Section 4.

It can also be observed that, when the undamaged configuration is symmetric with respect to 3-axis (single-fibre, θ_2=0º, 180º), even though the initial damage is located at α=135º (involving a loss of the symmetry), the interface crack achieves again a symmetric configuration at the end of the unstable growth. Finally, it is important to remark that, when the secondary fibre tends to be aligned with the direction of the external load, i.e. aligned with 2-axis, the final configuration debonded zone ('bubble') is slightly displaced towards the position of the secondary fibre (see θ_2=90º, 270º in Fig. 8).

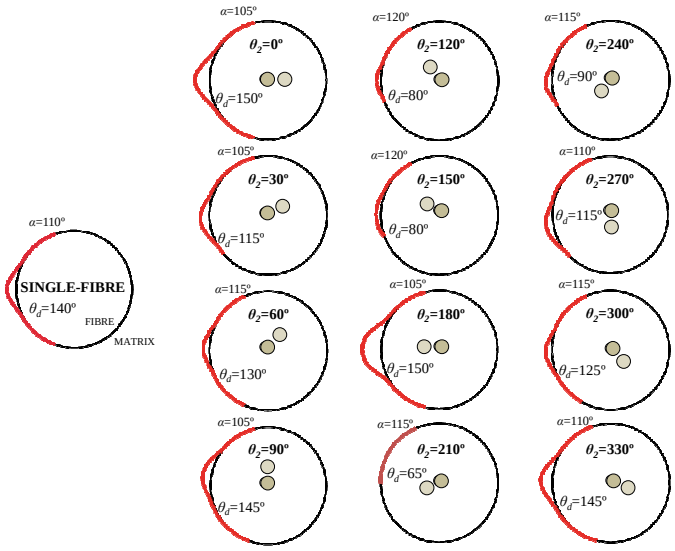

Fig. 8. Final deformed configurations of the interface crack for the single-fibre case and a selection of positions of the secondary fibre (c_f=0.5).

7. Conclusions

The most noteworthy conclusion for the non-frictional case is that when the secondary fibre is approximately aligned with the initial failure (105º≤θ_2≤150º) or at 120º from these positions (225º≤θ_2≤285º and 345º≤θ_2≤45º), its presence has an accelerative effect against the initiation of the crack growth; whereas for the rest of the positions, the presence of the secondary fibre has a protective effect. In relation to the increase of the inter-fibre spacing, the disappearance of the totality of the alterations produced by the nearby fibre occurs for r_2/r_2^0=4.

Regarding the effect of the presence of friction on the interface crack growth, the most general alteration observed on the single-fibre and two-fibre models, is the decrease of the level of the Energy Release Rate along the whole range of growth under consideration. Moreover, on the assumption that the crack grows at both crack tips, and despite the asymmetry of the initial damage, when the undamaged configuration is symmetric with respect to the axis perpendicular to the load, the final deformed configuration is also symmetric.

The θ_2 ranges for which the unstable growth achieves the largest lengths coincides approximately for the non-frictional and the frictional studies; the largest lengths of unstable growth are found when the position of the secondary fibre is perpendicular to the direction of the external load. However, this fact is not maintained for the shortest ranges of unstable growth: for the frictional case, these ranges are found when the secondary fibre is aligned with the location where the contact zones of both crack tips are expected to develop (in view of the single-fibre results), whereas for the non-frictional case, the shortest lengths of unstable growth are obtained when the secondary fibre is approximately aligned with the direction of the load or with the contact zone associated with the lower crack tip. In any case, the influence of the considerable decrease of the Energy Release Rate on the arresting criterion of the interface crack for the frictional case together with the both crack tips growth hypothesis, produce greater lengths of unstable growth when considering friction between the crack lips.

Acknowledgments

This work was supported by the Spanish Ministry of Education, Culture and Sports under Grants MAT2016-80879-P and MAT2013-45069-P.

References

[1] E. Correa, V. Mantič, and F. París. Numerical characterisation of the fibre–matrix interface crack growth in composites under transverse compression. *Engineering Fracture Mechanics,* 75: 4085-4103, 2008.
[2] E. Correa, V. Mantič, and F. París. A micromechanical view of inter-fibre failure of composite materials under compression transverse to the fibres. *Composites Science and Technology,* 68(9):2010-2021, 2008
[3] E. Correa, F. París and V. Mantič. Effect of a secondary transverse load on the inter-fibre failure under compression. *Composites Part B: Engineering*, 65:57-68, 2014.
[4] C. Sandino, E. Correa and F. París. Numerical analysis of the influence of a nearby fibre on the interface crack growth in composites under transverse tensile load. *Engineering Fracture Mechanics*, 168:58–75, 2016.
[5] C. Sandino, E. Correa and F. París. Composite materials under transverse biaxial loads: Study of the influence of a nearby fibre on the interface crack growth under tension. *ECCM 2016 - Proceeding of the 17th European Conference on Composite Materials, Munich, Germany,* June 26-30 2016.
[6] V. Mantič, A. Blázquez, E. Correa and F. París. Analysis of interface cracks with contact in composites by 2D BEM. In M. Guagliano and M.H. Aliabadi, editors. *Fracture and Damage of Composites*, Southampton: WIT Press, 189–248, 2006.
[7] E. Graciani, V. Mantič, F. París and A. Blázquez. Weak formulation of axi-symmetric frictionless contact problems with boundary elements. Application to interface cracks. *Comput Struct,* 83:836–855, 2005.
[8] G.R. Irwin. Analysis of stresses and strain near the end of a crack transversing a plate. *Journal of Applied Mechanics*, 24:361–364, 1957.
[9] V. Toya. A crack along the interface of a circular inclusion embedded in an infinite solid. *Journal of the Mechanics and Physics of Solids*, 22:325–348, 1974.
[10] Y. Murakami. *Stress Intensity Factor Handbook*. Oxford: Pergamon Press; 1988.
[11] J.W. Hutchinson and Z. Suo. Mixed mode cracking in layered materials. *Advances in Applied Mechanics*, 29:63–191, 1992.
[12] V. Mantič and F. París. Relation between SIF and ERR based measures of fracture mode mixity in interface cracks. *International Journal of Fracture*, 130:557–569, 2004.
[13] E. Graciani, V. Mantič, F. París, J. Varna . Fibre-Matrix debonding in composite materials: axial loading. In R Talreja and J Varna, editors. *Modeling damage, fatigue and failure of composite materials*, Cambridge: Woodhead Publishing, 7:117–141, 2016.